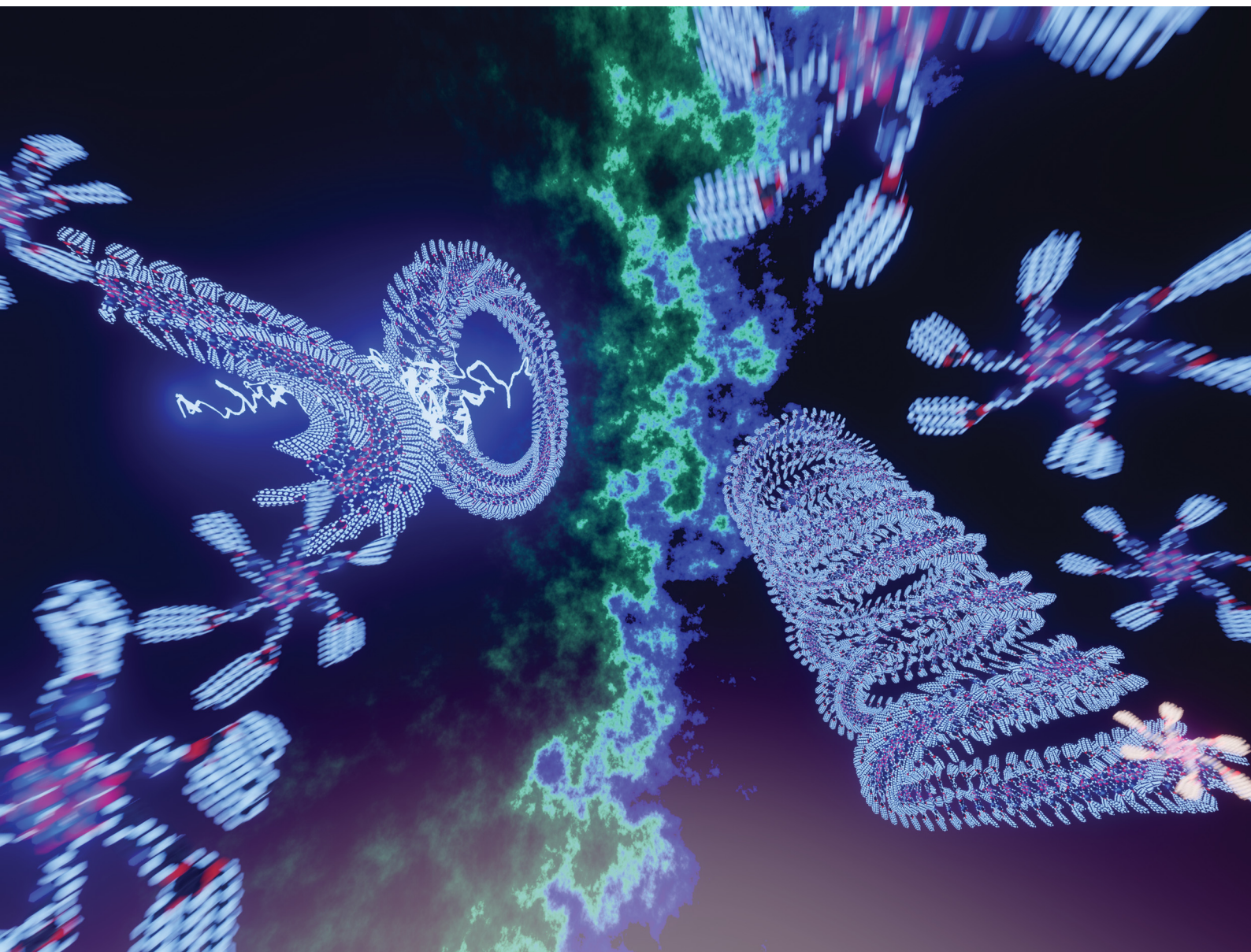


# ChemComm

Chemical Communications

[rsc.li/chemcomm](https://rsc.li/chemcomm)



ISSN 1359-7345

**COMMUNICATION**

Shiki Yagai *et al.*

Distinct seed topologies enable comparison of elongation and secondary nucleation pathways in seeded supramolecular polymerization





Cite this: *Chem. Commun.*, 2023, 59, 7375

Received 31st March 2023,  
Accepted 24th April 2023

DOI: 10.1039/d3cc01587d

rsc.li/chemcomm

# Distinct seed topologies enable comparison of elongation and secondary nucleation pathways in seeded supramolecular polymerization†

Hiroki Itabashi,<sup>a</sup> Keigo Tashiro, <sup>b</sup> Shumpei Koshikawa,<sup>a</sup> Sougata Datta <sup>c</sup> and Shiki Yagai <sup>\*cd</sup>

**The influence of seed topologies on seeded supramolecular polymerization was examined using helicoidal and toroidal supramolecular polymer seeds. The addition of these seeds to a supersaturated solution of monomers led to distinct nucleation-growth kinetics, which were attributed to the significant difference between the elongation from helicoid termini and secondary nucleation catalyzed by the toroid surface.**

Supramolecular polymer (SP) research has witnessed remarkable progress over the last two decades.<sup>1</sup> One of the most important advancements is seeded supramolecular polymerization methodology, which has been extensively investigated in the past decade.<sup>2</sup> In this approach, monomers are assembled into metastable structures<sup>3</sup> or organized into dormant monomer conformations<sup>4</sup> that are unlikely to undergo spontaneous nucleation. The addition of seeds to this “supersaturated” monomer solution initiates supramolecular polymerization by activating the deactivated monomers. Although seeded supramolecular polymerization has been achieved by using a variety of specifically designed monomers,<sup>2–4</sup> further development of this method requires a deeper understanding with a more sophisticated self-assembly process.

Another closely associated phenomenon is surface-catalyzed secondary nucleation, which is believed to be an important process in the formation mechanism of amyloid fibrils.<sup>5</sup> In this event, monomers preferentially nucleate on the surface of co-existing aggregates like seeds through weak interactions

such as hydrophobic effects and van der Waals forces. Although secondary nucleation should contribute more or less to seeded polymerization, it is difficult to differentiate seed-induced elongation and secondary nucleation in ordinary supramolecular polymer systems with growth competent ends.<sup>2–4</sup> As an exception, George and co-workers showed distinct kinetics in the stereoselective induction of seed-induced elongation and secondary nucleation pathways in a one-dimensional supramolecular polymer system.<sup>6</sup>

In this study, we exploit the topological features of our unique supramolecular polymer systems with intrinsic curvature to compare the impact of terminal elongation and secondary nucleation–elongation in seeded supramolecular polymerization. We have explored the self-assembly of a series of barbituric acid monomers with a  $\pi$ -conjugated core and aliphatic tail such as **1** (Fig. 1a).<sup>7</sup> These monomers, upon cooling their molecularly dissolved hot solutions in a nonpolar solvent, nucleate through hexamerization of monomers (rosette formation) by hydrogen bonding and subsequently stacking of rosettes by  $\pi$ – $\pi$  interaction (Fig. 1b). The following elongation with the generation of intrinsic curvature produces various curved structures depending on self-assembly conditions. For example, toroidal supramolecular polymers (**SP**<sub>ring</sub>) and open-ended randomly coiled supramolecular polymers (**SP**<sub>random</sub>) are obtained under kinetic conditions such as fast cooling, while helicoidal supramolecular polymers (**SP**<sub>helicoid</sub>) are formed under thermodynamic conditions such as slow cooling (Fig. 1c).<sup>7c</sup> Furthermore, we have succeeded in creating nano-polycatenanes by realizing a topological hierarchical organization of **SP**<sub>ring</sub> using secondary nucleation.<sup>8a,b</sup> With these topologically regulated supramolecular polymers in hand, we envisioned that we could compare the kinetics of terminal elongation and secondary nucleation of the same molecule using open-ended **SP**<sub>helicoid</sub> and the closed-ended **SP**<sub>ring</sub> as seeds.

To examine the above idea, we had to fulfill two requirements simultaneously: one is that monomers have to be trapped in a supersaturated state instead of spontaneous nucleation and the other is that the added seeds are kinetically

<sup>a</sup> Division of Advanced Science and Engineering, Graduate School of Science and Engineering, Chiba University, 1-33 Yayoi-cho, Inage-ku, Chiba 263-8522, Japan

<sup>b</sup> Department of Applied Chemistry, Faculty of Science and Technology, Seikei University, 3-3-1 Kichijoji-kitamachi, Musashino-shi, Tokyo, 180-8633, Japan

<sup>c</sup> Institute for Advanced Academic Research (IAAR), Chiba University, 1-33 Yayoi-cho, Inage-ku, Chiba 263-8522, Japan. E-mail: yagai@faculty.chiba-u.jp

<sup>d</sup> Department of Applied Chemistry and Biotechnology, Graduate School of Engineering, Chiba University, Chiba 263-8522, Japan

† Electronic supplementary information (ESI) available. See DOI: <https://doi.org/10.1039/d3cc01587d>





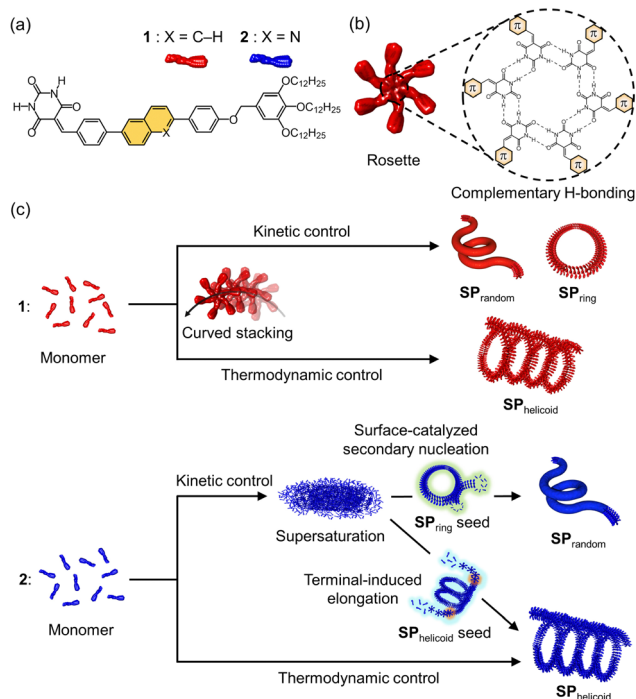


**Fig. 1** (a) The molecular structures of **1** and **2**. (b) A schematic representation of a hydrogen-bonded cyclic hexamer (rosette). (c) A schematic representation of the supramolecular polymerization processes of **1** and **2** depending on the self-assembly kinetics and seed topologies for **2**.

stable so that they do not feed monomers. With our previously reported molecule **1**, spontaneous nucleation could be delayed by keeping a monomeric solution just below the nucleation temperature (*ca.* 330 K for solutions with a concentration around  $10^{-5}$  M) in methylcyclohexane (MCH) or by quenching a hot monomer solution in a MCH-toluene mixture.<sup>8</sup> Although the SP<sub>ring</sub> of **1** is stable under these supersaturated conditions,<sup>8a,b</sup> the corresponding SP<sub>helixoid</sub> is depolymerized due to the presence of termini. On the other hand, it is difficult to prepare a supersaturated solution of **1** under conditions where SP<sub>helixoid</sub> is kinetically stable. With these contradictory requirements in mind, we rationally designed the new molecule **2** with a  $\pi$ -electron deficient quinoline unit that is expected to assemble more weakly than **1**, and thereby its spontaneous nucleation is suppressed enough even under conditions where SP<sub>helixoid</sub> is not depolymerized. Here, we report distinctly different effects of SP<sub>helixoid</sub> and SP<sub>ring</sub> seeds on the supramolecular polymerization kinetics of **2** in its supersaturated solution (Fig. 1c).

Compound **2** was synthesized and characterized using <sup>1</sup>H and <sup>13</sup>C NMR spectroscopies and ESI- and APCI-MS spectrometry (Scheme S1 and Charts S1–S8, ESI†). To study how the quinoline heterocyclic core could electronically affect the aggregation of **1**, we conducted density functional theory (DFT) calculations of **1** and **2** with the basis set of B3LYP/6-31G(d) in MCH. Visualization of the molecular electrostatic potential revealed that the negative charge is localized on the N atom in the quinoline unit of **2** because of the lone pair, while the naphthalene in **1** rarely possesses charge (Fig. S1a, ESI†). The permanent dipole moment

of **2** (4.68 D) is smaller than that of **1** (7.91 D) because the negative charge in the quinoline unit neutralizes the electron-withdrawing effect of the barbituric acid unit (Fig. S1b, ESI†). From these calculations, we expected that the N atom of the quinoline unit weakened the  $\pi$ - $\pi$  aggregation of **2** due to the weak permanent dipole moment.

Upon cooling a hot monomeric MCH solution of **2** ( $c = 5.0 \times 10^{-6}$  M) at a rate of  $1.0 \text{ K min}^{-1}$ , the absorption band of the diphenylquinoline chromophore showed a bathochromic shift from 394 to 404 nm with a concomitant increase in the absorption intensity at around 470 nm (Fig. S2a, ESI†). This spectral change is typical of the formation of J-type stacking of barbiturate  $\pi$ -conjugated systems. Monitoring the growth of the absorption intensity at 470 nm upon cooling revealed a non-sigmoidal aggregation curve, suggesting a cooperative supramolecular polymerization process (Fig. S2b, ESI†). When the resulting solution was spin-coated onto highly oriented pyrolytic graphite (HOPG), atomic force microscopy (AFM) showed SP<sub>helixoid</sub> similar to those observed for **1** (Fig. S3b and c, ESI†).<sup>7c</sup> After aging the solution at 293 K for 1 day, the absorption spectrum of **2** showed a hypochromic change (Fig. S3a, ESI†), which is most likely due to higher-order folding as shown by AFM (Fig. S3d and e, ESI†).<sup>7c</sup>

The thermodynamic parameters of the equilibrated 1-day aged SP<sub>helixoid</sub> of **2** were estimated by temperature-dependent absorption measurements for different concentrations upon heating and using modified van't Hoff analysis (Fig. S4, ESI†). We obtained the standard enthalpy ( $\Delta H^\circ$ ) of  $-147 \text{ kJ mol}^{-1}$ , standard entropy ( $\Delta S^\circ$ ) of  $-306 \text{ kJ mol}^{-1} \text{ K}^{-1}$ , and standard Gibbs free energy change ( $\Delta G^\circ$ ) of  $-56 \text{ kJ mol}^{-1}$  at 298 K. Comparing these parameters to those of the fully folded SP<sub>helixoid</sub> of **1** ( $\Delta H^\circ = -176 \text{ kJ mol}^{-1}$ ,  $\Delta S^\circ = -383 \text{ kJ mol}^{-1} \text{ K}^{-1}$ , and  $\Delta G^\circ = -62 \text{ kJ mol}^{-1}$ ) demonstrates that the SP<sub>helixoid</sub> of **2** contains weaker intermolecular interactions than **1**.<sup>7c</sup> This result is in line with the difference of the permanent dipole moment between **1** and **2** based on the DFT calculations.

Supramolecular polymerization of our barbiturate monomers is strongly influenced by the solvent properties.<sup>9</sup> In our previous study of **1**, adding an aromatic solvent like toluene as a co-solvent to nonpolar MCH solutions of **1** effectively retarded spontaneous nucleation due to solvation of the  $\pi$ -surface of the rosettes, which enables rearrangement to a variety of other hydrogen-bonded aggregates.<sup>8c</sup> To study the effect of toluene on the supramolecular polymerization of **2**, we measured the thermal hysteresis between the cooling and heating curves. In pure MCH, a small thermal hysteresis was observed upon immediately heating the as-cooled MCH solution of **2** at a rate of  $1.0 \text{ K min}^{-1}$  (Fig. 2a). The difference in the temperature at which 50% of monomers aggregate between the heating and cooling curves ( $\Delta T_{50} = T_{50\text{-heating}} - T_{50\text{-cooling}}$ ) was 6.0 K in pure MCH. In contrast, a significantly larger  $\Delta T_{50}$  of 20.5 K was observed in the toluene/MCH (40/60 (v/v)) mixture (Fig. 2b). The hysteresis loop suggests that spontaneous nucleation of **2** is also effectively retarded due to the formation of diverse hydrogen-bonded species.

Based on the above observation, we expected that quicker cooling in the toluene/MCH mixture could further suppress spontaneous nucleation even at practical temperatures, which



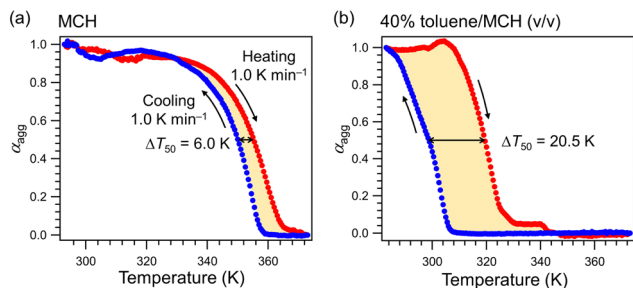


**Fig. 2** (a) and (b) Cooling (blue) and heating (red) curves of **2** ( $c = 2.0 \times 10^{-5}$  M) obtained by plotting the mole fraction of the aggregated molecules ( $\alpha_{\text{agg}}$ , calculated from the absorption change at 470 nm) as a function of temperature in pure MCH (a) and in 40% toluene/MCH (v/v) (b). Note that the second dissociation step around 340 K in (b) is due to **SP**<sub>ring</sub>.

allows us to conduct seeding experiments. Upon rapidly cooling ( $10 \text{ K min}^{-1}$ ) a hot monomeric 40% toluene/MCH (v/v) solution of **2** from 373 to 293 K, no absorption increase around 470 nm was observed, while the absorption band showed a hyperchromic effect with a small red shift due to planarization of the molecules.<sup>10</sup> This suggests that spontaneous nucleation of **2** was successfully suppressed at room temperature (Fig. 3a and Fig. S5, ESI<sup>†</sup>). For such a supersaturated solution, AFM imaging showed no well-defined mesoscopic assemblies (Fig. 3b). Upon aging, the red-shifted absorption band characteristic of aggregated **2** grew over 2000 s (Fig. 3a), which was accompanied by the formation of large assemblies over 100 nm as confirmed by dynamic light scattering (DLS, Fig. 3c). AFM analysis after equilibration showed the formation of folded **SP**<sub>helixoid</sub> (Fig. 3d and Fig S6, ESI<sup>†</sup>). Thus, the supersaturated solution

obtained by rapid cooling is suitable to conduct seeded supramolecular polymerization under ambient conditions.

Having obtained the supersaturated solution in the 40% toluene/MCH (v/v) mixture, we investigated the impact of seed topologies for self-assembly kinetics. For this purpose, we prepared pure samples of short **SP**<sub>helixoid</sub> and **SP**<sub>ring</sub>. A short-**SP**<sub>helixoid</sub> solution of **2** could be prepared by applying sonication to an elongated-**SP**<sub>helixoid</sub> solution prepared in pure MCH (Fig. S7, ESI<sup>†</sup>). AFM images suggest that the column length of the short **SP**<sub>helixoid</sub> is *ca.* 100–200 nm. The solvent was replaced with a 40% toluene/MCH (v/v) mixture to avoid any changes in the final solvent composition. There was no change in the absorption spectra after sonication and addition of the solvent (Fig. S8, ESI<sup>†</sup>), suggesting that the **SP**<sub>helixoid</sub>-seeds remained intact. On the other hand, a **SP**<sub>ring</sub>-seed solution can be prepared using a judicious protocol that takes advantage of their thermal stability derived from their close-ended robust structure.<sup>8a,b</sup> In brief, open-ended short fibers in a **SP**<sub>ring</sub>-rich solution obtained by injecting a monomeric chloroform solution of **2** into MCH were thermally reorganized into the elongated **SP**<sub>helixoid</sub>. Filtration using a 200 nm porous membrane filter provided a pure **SP**<sub>ring</sub> solution (Fig. S9, ESI<sup>†</sup>). For this sample, the MCH solvent was also replaced with a 40% toluene/MCH (v/v) mixture by evaporation under reduced pressure and re-dissolution.

Seeding experiments were conducted on the supersaturated solution of **2** ( $c = 1.0 \times 10^{-5}$  M) using the above **SP**<sub>helixoid</sub>- and **SP**<sub>ring</sub>-seed solutions ( $c = 1.0 \times 10^{-5}$  M), respectively (Fig. 4a). Fig. 4b shows the effects of the seed topologies on the nucleation kinetics of the supersaturated solution. Compared to the

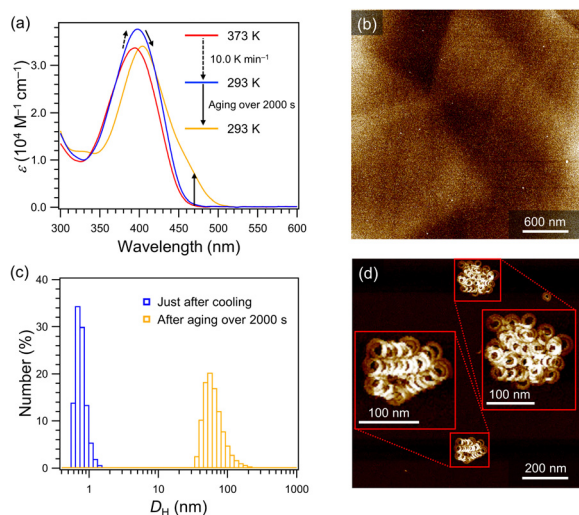


**Fig. 3** (a) Temperature- and time-dependent absorption spectral changes of **2** ( $c = 1.0 \times 10^{-5}$  M) in 40% toluene/MCH (v/v). (b) The AFM image of a sample prepared from the supersaturated solution of **2** ( $c = 1.0 \times 10^{-5}$  M) in 40% toluene/MCH (v/v). (c) DLS profiles of a 40% toluene/MCH (v/v) solution of **2** ( $c = 1.0 \times 10^{-5}$  M) just after cooling (blue bars) and after aging over 2000 s (orange bars) at 293 K. (d) The AFM image of **SP**<sub>helixoid</sub> obtained from the 40% toluene/MCH (v/v) solution of **2** ( $c = 1.0 \times 10^{-5}$  M) after aging for 2000 s at 293 K.

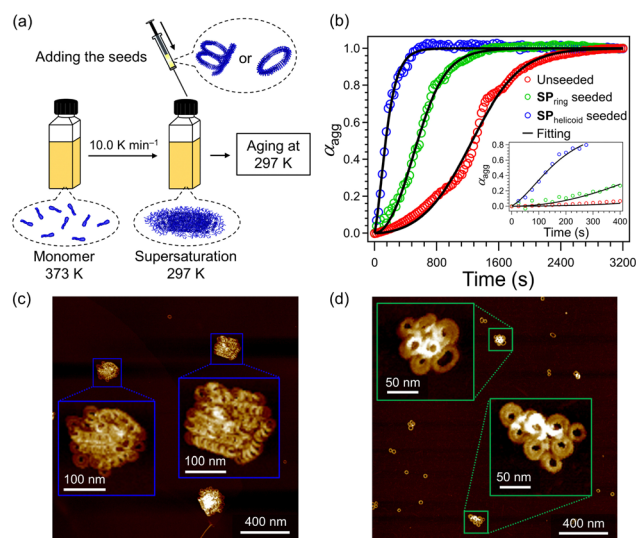


**Fig. 4** (a) Depiction of the seeded supramolecular polymerization protocol. (b) Time-dependent changes in the molar fraction of aggregated **2** ( $\alpha_{\text{agg}}$ , calculated from the absorption change at 470 nm) in a supersaturated solution in 40% toluene/MCH solution ( $c = 1.0 \times 10^{-5}$  M) at 297 K without any seeds (red curve) and with **SP**<sub>helixoid</sub> seeds (blue) ( $c = 1.0 \times 10^{-5}$  M) or **SP**<sub>ring</sub> seeds (green) ( $c = 1.0 \times 10^{-5}$  M). Inset: Time-dependent changes at the initial stage (0–400 s). (c) and (d) AFM images of supramolecular polymers obtained by the **SP**<sub>helixoid</sub>-seeded (c) and **SP**<sub>ring</sub>-seeded (d) solutions, respectively.



sigmoidal growth curve of the unseeded solution (red plot), the concave growth curve was recorded for the  $\text{SP}_{\text{helicoioid}}$ -seeded solution (blue plot). The concave growth curve suggests that the active ends of the  $\text{SP}_{\text{helicoioid}}$  seeds recruit supersaturated monomers and induced elongation of the  $\text{SP}_{\text{helicoioid}}$  seeds just after the addition. AFM observation after equilibration showed the formation of the elongated  $\text{SP}_{\text{helicoioid}}$  with columnar lengths over 500 nm, which further demonstrates that elongation occurred continuously from the termini of the  $\text{SP}_{\text{helicoioid}}$  seeds (Fig. 4c and Fig. S10, ESI†). The elongation kinetics could be fitted with the seed-induced nucleation elongation model in Amylofit software.<sup>11</sup> The primary nucleation and elongation rate constant ( $k_p k_n$ ) was estimated to be  $73 \text{ M}^{-1.3} \text{ s}^{-2}$ , which was significantly larger than that of the unseeded solution ( $k_p k_n = 0.68 \text{ M}^{-1.3} \text{ s}^{-2}$ ) estimated by fitting with the unseeded secondary nucleation elongation model (Table S1, ESI†).

In sharp contrast to the above  $\text{SP}_{\text{helicoioid}}$ -seeded experiment, the accelerated sigmoidal growth curve was recorded for the  $\text{SP}_{\text{ring}}$ -seeded solution (green plot, Fig. 4b). The growth curve in the presence of  $\text{SP}_{\text{ring}}$  seeds was accurately represented by the secondary nucleation elongation model and the reaction order of secondary nucleation ( $n_2$ ) in the  $\text{SP}_{\text{ring}}$ -seeded system resulted in 1.4, which was larger than the 0.9 of the unseeded system (Table S1, ESI†). The sigmoidal curve illustrates that the growth rate increased despite the decreasing monomer concentration, which cannot be explained by elongation alone and suggests the formation of new aggregates.<sup>5a</sup> Notably, AFM observation of the  $\text{SP}_{\text{ring}}$ -seeded solution after equilibration showed  $\text{SP}_{\text{random}}$ , which was hardly observed in the  $\text{SP}_{\text{helicoioid}}$ -seeded experiment (Fig. 4d and Fig. S11, ESI†). The monomer distribution ratio between  $\text{SP}_{\text{random}}$  and  $\text{SP}_{\text{ring}}$  was 42:58 (Fig. S12, ESI†), which suggests that the newly generated products by secondary nucleation were mostly  $\text{SP}_{\text{random}}$ . These kinetics and AFM observation demonstrate that the  $\text{SP}_{\text{ring}}$  indeed has no terminal ends and acts as an active surface for secondary nucleation.

In conclusion, our unique open- and closed-ended SPs allowed us to demonstrate the distinct kinetics of secondary nucleation and elongation on seeded supramolecular polymerization. Our seeded experiments using two types of seeds with or without terminal ends, respectively, clearly demonstrated that the open-ended  $\text{SP}_{\text{helicoioid}}$ -seeds induced terminal-elongation whereas the closed-ended  $\text{SP}_{\text{ring}}$ -seeds induced secondary nucleation on the surface of SPs covered with peripheral alkyl chains. Hence, the elongated  $\text{SP}_{\text{helicoioid}}$  was exclusively obtained by elongation from co-existing  $\text{SP}_{\text{helicoioid}}$  seeds, whereas the sole occurrence of secondary nucleation on  $\text{SP}_{\text{ring}}$  seeds at room temperature afforded random coil structures. Further development of these techniques will enable precise construction of different supramolecular topologies and interlocked self-assemblies.

This work was supported by the Japan Society for the Promotion for Science (JSPS) KAKENHI grant no. 22H00331,

22K20526, and 23H04873 in a Grant-in-Aid for Transformative Research Areas "Materials Science of Meso-Hierarchy". S. Y. acknowledges financial support from The Mitsubishi Foundation (grant no. 202110037).

## Conflicts of interest

There are no conflicts to declare.

## Notes and references

- (a) L. Brunsveld, B. J. B. Folmer, E. W. Meijer and R. P. Sijbesma, *Chem. Rev.*, 2001, **101**, 4071; (b) T. F. A. De Greef, M. M. J. Smulders, M. Wolffs, A. P. H. J. Schenning, R. P. Sijbesma and E. W. Meijer, *Chem. Rev.*, 2009, **109**, 5687; (c) T. Aida, E. W. Meijer and S. I. Stupp, *Science*, 2012, **335**, 813.
- S. Ogi, K. Sugiyasu, S. Manna, S. Samitsu and M. Takeuchi, *Nat. Chem.*, 2014, **6**, 188.
- (a) J. S. Valera, R. Gómez and L. Sánchez, *Small*, 2018, **14**, 1702437; (b) K. Jalani, A. D. Das, R. Sasnal, S. S. Agasti and S. J. George, *Nat. Commun.*, 2020, **11**, 3967; (c) J. Matern, Z. Fernández, N. Bäumer and G. Fernández, *Angew. Chem., Int. Ed.*, 2022, **61**, e202203783; (d) W. Wagner, M. Wehner, V. Stepanenko and F. Würthner, *J. Am. Chem. Soc.*, 2019, **141**, 12044; (e) T. Fukui, S. Kawai, S. Fujinuma, Y. Matsushita, T. Yasuda, T. Sakurai, S. Seki, M. Takeuchi and K. Sugiyasu, *Nat. Chem.*, 2017, **9**, 493; (f) M. Wehner, M. I. S. Röhr, M. Bühler, V. Stepanenko, W. Wagner and F. Würthner, *J. Am. Chem. Soc.*, 2019, **141**, 6092; (g) A. J. Markvoort, H. M. M. ten Eikelder, P. A. J. Hilbers and T. F. A. de Greef, *ACS Cent. Sci.*, 2016, **2**, 232.
- (a) S. Ogi, V. Stepanenko, K. Sugiyasu, M. Takeuchi and F. Würthner, *J. Am. Chem. Soc.*, 2015, **137**, 3300; (b) M. Endo, T. Fukui, S. H. Jung, S. Yagai and M. Takeuchi, *J. Am. Chem. Soc.*, 2016, **138**, 14347; (c) O. Shyshov, S. V. Haridas, L. Pesce, H. Qi, A. Gardin, D. Bochicchio, U. Kaiser, G. M. Pavan and M. von Delius, *Nat. Commun.*, 2021, **12**, 3134; (d) Q. Huang, N. Cissé, M. C. A. Stuart, Y. Lopatina and T. Kudernac, *J. Am. Chem. Soc.*, 2023, **145**, 5053; (e) H. Choi, S. Ogi, N. Ando and S. Yamaguchi, *J. Am. Chem. Soc.*, 2021, **143**, 2953; (f) E. E. Greciano, S. Alsina, G. Ghosh, G. Fernández and L. Sánchez, *Small Method*, 2020, **4**, 1900715; (g) N. Fukaya, S. Ogi, M. Kawashiro and S. Yamaguchi, *Chem. Commun.*, 2020, **56**, 12901.
- (a) S. I. A. Cohen, M. Vendruscolo, C. M. Dobson and T. P. J. Knowles, *J. Mol. Biol.*, 2012, **421**, 160–171; (b) T. Sinnige, *Chem. Sci.*, 2022, **13**, 7080.
- S. Sarkar, A. Sarkar, A. Som, S. S. Agasti and S. J. George, *J. Am. Chem. Soc.*, 2021, **143**, 11777.
- (a) S. Yagai, Y. Kitamoto, S. Datta and B. Adhikari, *Acc. Chem. Res.*, 2019, **52**, 1325; (b) S. Datta, S. Takahashi and S. Yagai, *Acc. Mater. Res.*, 2022, **3**, 259; (c) D. D. Prabhu, K. Aratsu, Y. Kitamoto, H. Ouchi, T. Ohba, M. J. Hollamby, N. Shimizu, H. Takagi, R. Haruki, S. Adachi and S. Yagai, *Sci. Adv.*, 2018, **4**, eaat8466.
- (a) S. Datta, Y. Kato, S. Higashihara, K. Aratsu, A. Isobe, T. Saito, D. D. Prabhu, Y. Kitamoto, M. J. Hollamby, A. J. Smith, R. Dalgliesh, N. Mahmoudi, L. Pesce, C. Perego, G. M. Pavan and S. Yagai, *Nature*, 2020, **583**, 400; (b) H. Itabashi, S. Datta, R. Tsukuda, M. J. Hollamby and S. Yagai, *Chem. Sci.*, 2023, **14**, 3270; (c) A. Isobe, D. D. Prabhu, S. Datta, T. Aizawa and S. Yagai, *Chem. – Eur. J.*, 2020, **26**, 8997.
- (a) M. F. J. Mabeoone, A. R. A. Palmans and E. W. Meijer, *J. Am. Chem. Soc.*, 2020, **142**, 19781; (b) Z. Chen, B. Fimmel and F. Würthner, *Org. Biomol. Chem.*, 2012, **10**, 5845; (c) G. Ghosh and S. Ghosh, *Chem. Commun.*, 2018, **54**, 5720.
- N. Bäumer, K. K. Kartha, N. K. Allampally, S. Yagai, R. Q. Albuquerque and G. Fernández, *Angew. Chem., Int. Ed.*, 2019, **58**, 15626.
- G. Meisl, J. B. Kirkegaard, P. Arosio, T. C. T. Michaels, M. Vendruscolo, C. M. Dobson, S. Linse and T. P. J. Knowles, *Nat. Protoc.*, 2016, **11**, 252.

